Real-time Observation of the Electrode-Size-Dependent Evolution Dynamics of the Conducting Filaments in CBRAM

Fang Yuan[†‡], Zhi Zhang[†], Chunru Liu[†], Feichi Zhou[†], Hei Man Yau[†], Wei Lu[†], Xiaoyan Qiu[†], H.–S. Philip Wong[†‡], Jiyan Dai[†], and Yang Chai[†]*

[†] Department of Applied Physics, The Hong Kong Polytechnic University, Hung Hom, Kowloon, Hong Kong, P. R. China

[‡] Department of Electrical Engineering and Stanford SystemX Alliance, Stanford University, Stanford, CA 94305, USA

ABSTRACT- Conducting Bridge Random Access Memory (CBRAM) is among the most promising candidates for future non-volatile memories. It is important to understand the scalability and retention of CBRAM cells to realize better memory performance. Here we directly observe the switching dynamics of Cu/SiO_2/W cells with various active electrode sizes using *in-situ* transmission electron microscopy. The conducting filaments (CFs) grow from the active electrode to inert electrode during the SET operations. The size of the active electrode affects the electric-field distribution, the amount of the cations injection into electrolyte, and the dimension of the CF, which further determines the power consumption and retention of the CBRAM cell. We also construct a theoretical model to explain the electrode-size-dependent CF growth in SET operations, showing good agreement with our experimental results.

KEYWORDS: *filament size, in-situ TEM, electrode-size-dependent CF growth, CBRAM*

TOC graphic:

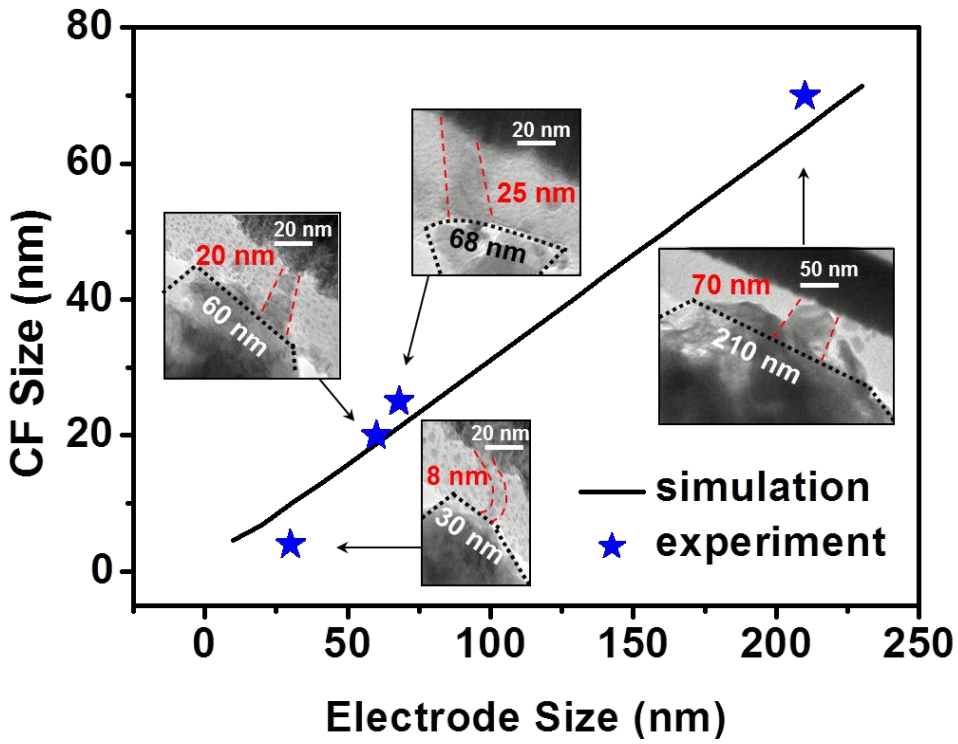

In the recent decades, resistive switching memory has been intensively investigated as one of the most promising next-generation non-volatile memories.[1-5] Conducting bridge random access memory (CBRAM) shows superior performance in terms of switching speed, power consumption, dimensional scalability and CMOS process compatibility.[5-10] CBRAM relies on the formation and rupture of metallic conductive filaments (CFs) to achieve repeatable switching between high resistance state (HRS) and low resistance state (LRS).[1, 11-13] This model has been supported by direct observations of the metal filaments in the CBRAM.[14-16] The performance of CBRAM critically depends on the size and morphology of the metal filament. It is of fundamental interest for researchers to understand the metal atom/ion migration which affects the scalability and performance of the CBRAM cell.

Generally, the CF growth in a CBRAM device exhibits randomness and is described by complex parameters.[16] Many researchers aim to control the CF location or avoid the over-injection of metal atoms/ions for realizing controllable switching. To control the location of CF growth, Liu *et al.* embedded several Cu nanocrystals inside the ZrO_2 electrolyte to provide a nucleus for the CF,[17] which guides a specific location for the CF formation and rupture processes, thereby improving the stability and uniformity of the memory. You *et al.* fabricated an Ag nanocone/SiO_2 nanomesh/Pt device by nanotransfer printing.[18] The nanocone-shaped Ag electrodes act as electric-field concentrator arrays and realize a selective and controllable CF growth, leading to significantly decreased variation in the switching characteristics. Over-injection of the atoms/ions into the dielectric not only leads to the variation of the CF size and location, but also results in wide or large number of CFs that causes current overshoot of the CBRAM switching operation. To limit the over-injection, Park *et al.* proposed a single-filament Cu/HfO_2/Pt CBRAM device, in which the Cu electrode is removed after the forming process.[19, 20] By activating a single filament, the variation of CBRAM device is greatly reduced. In other works, graphene has been employed for blocking excessive atoms/ions from moving into the dielectrics,[21,22] which may be a potential method to localize and limit the filaments inside CBRAM cells.

In this work, we perform real-time observations of the CF formation and dissolution processes during electrical switching for a typical CBRAM device using *in-situ* transmission electron microscopy (TEM). By changing the size of the active electrode tip in the memory cell, the metal

ions injection can be modified, resulting in different sizes of the CF. A theoretical model is developed to explain the electrode-size-dependent CF growth. This understanding of the origin of the CF evolution will help guide the design of future CBRAM devices.

Results and discussions

Figure 1a illustrates the schematic of the *in-situ* TEM measurement set-up. The TEM specimen was fixed onto the Cu grid by silver paste inside the Nanofactory^{TM} STM-holder. The W bottom electrode (BE) of the memory device was connected to a source meter through an electrical cable. A Cu tip was installed on a piezo-driven hat. The Cu wire was contacted to the surface of the SiO_2 film to form a Cu/SiO_2/W CBRAM device. During the electrical measurements, an electrical bias was applied to the movable Cu tip respect to the fixed TEM grid holder. **Figure 1**b shows the *I-V* curve of the device measured inside the TEM. Compared to the *ex-situ* measured *I-V* curves (Figure S1 in **Supporting Information**), the device also exhibits a bipolar switching behavior, where a positive bias triggers the cell to LRS, and a negative bias enables RESET process.

Figure 1c shows the corresponding TEM image of the device after the SET process. We can clearly observe that a dark bridge-like region (marked with red dash lines) within the SiO_2 layer connects the Cu tip and the W electrode, which confirms the formation of a filament. The filament exhibits an inverted cone-shape with the diameter of ~14 nm close to Cu tip and a relatively smaller size of ~10 nm near W BE. Because Cu ion has relatively low mobility in SiO_2 compared to that in electrolytes like Cu-GeTe, Ta_2O_5, the rate limiting factor of the filament growth is the cation supply instead of reduction rates.[23] During the CF growth, the Cu ions preferably migrate to, and get reduced at the leading edge of the existing Cu filament. As a result, an inverted cone-shaped CF is established, which is also in good agreement with previous reports.[23]

It is noteworthy that the CF in LRS is in the shape of a chain of nanoclusters with certain gaps instead of a continuous bridge. With the narrow Cu tip, only a small amount of Cu is injected into SiO_2 in the form of nanocluster. Due to the low and inhomogeneous ion mobility, the Cu ions agglomerate, get reduced and nucleate along a path with the highest defect density and

lowest electrochemical potentials inside the dielectrics. Therefore, the subsequent filament growth is in the form of clusters and has a curved shape.[16]

The CF is unstable and gradually dissolves after the SET operations, as shown in the *in-situ* TEM images in Figure S2 **(Supporting Information)**. The devices show poor retention for the LRS. One possible reason is insufficient Cu ions migrated into SiO_2 to form wide and robust CF. Takahashi *et al.* also reported LRS failure in a 30-nm CBRAM device with SET current lower than 40 μA. The CF was almost invisible in TEM images and the LRS was kept for less than 1000 seconds.[24] Furthermore, Guy *et al.* reported that, for the memory cell less than 10 nm, the LRS device with thinner CF (the thin CF size was obtained by a soft SET operation) exhibited quite unstable retention properties due to the lateral Cu diffusion from the CF.[25] The operation current is smaller for a CBRAM device with a narrower CF and leads to lower power consumption. Therefore, a trade-off between the data retention and power consumption must be carefully considered for the design of CBRAM.

After the negative RESET sweep, the dark bridge region of CF is ruptured, and some residual Cu clusters remain at the Cu/SiO_2 interface, as shown in **Figure 1**d. These remaining Cu clusters provide seeds for the subsequent SET cycle, where the Cu ions migrate to the leading edge, and the CF gradually grows towards the inert W cathode.[12, 14] **Figure 1**e shows energy-dispersive X-ray spectroscopy (EDX) of the device at LRS and HRS. Weak Cu signal was detected in the HRS in the SiO_2 films, which mainly comes from the Cu grid holder. In contrast, a much stronger Cu signal was present in the LRS, providing solid evidence of the formation of Cu filament.

By varying the Cu tip contact area to the SiO_2 surface, the size of active Cu electrode can be changed. The local electrical field distribution and Cu cation supply during the SET process are both affected by the size of active Cu electrode. **Figure 2**a-b and **Figure 3**a-b show the *in-situ I-V* curves and the corresponding CF growth dynamics with four different active electrode sizes. Each subfigure comprises a series of TEM images that are extracted from videos Movie S1-S4 (**Supporting Information**) corresponding to the states marked in the *I-V* curves.

In **Figure 2**a, the diameter of the Cu tip close to the SiO_2 is around 30 nm. State I is the HRS of the device. With the bias sweep to +14 V, no obvious change is observed (8 s in Movie S1,

Supporting Information). A dark region suddenly appears when the bias is swept to +16 V. The existing Cu nanocluster starts to enlarge, indicating more Cu atoms migrated into the SiO_2 (state II and III). During this state, the current gradually increases to ~μA level. With the increase of bias, more and more nanoclusters emerged inside the oxide layer close to one another, and gradually grow in a curved path toward the inert W electrode. When the sweep bias reaches +25 V, the nanoclusters finally form the shape of a curved CF with a diameter of 8 nm in the widest part. Simultaneously, the current reaches to a highest level of ~10 μA, suggesting the device was SET to LRS (state IV). In **Figure 2**b, a Cu tip with the diameter of about 60 nm contacts to SiO_2. The device is SET at the bias of +18 V, and a CF with the diameter of 20 nm in the widest part is formed. The CF is in the shape of an inverted cone comprising of several nanoclusters with gaps between each cluster.

These nanoclusters can be considered as bipolar electrodes under an electrical field.[16] **Figure 2**c depicts the starting state without external bias. Some Cu atoms have been driven into SiO_2 at the interface due to the previous switching cycles. Under the electrical field as shown in **Figure 2**d, Cu cations are generated at the virtual anode side (δ+) of one cluster and drift along the electrical field, and then get reduced at the virtual cathode side (δ-) of another cluster, resulting in an effective cluster displacement along the electric field. Only limited Cu atoms are injected into SiO_2 to form a thin CF due to the small Cu electrodes. These thin filaments have relative high surface energy.[26] The thermodynamically energy favored sites for the thin CF are largely determined by the inhomogeneous dielectrics. Therefore, the CF in devices with small electrode tends to stay in the shape of thin and discrete clusters, as illustrated in **Figure 2**e.

With the increase of Cu tip size, the CF exhibits different characteristics. **Figure 3**a shows the *in-situ I-V* curve and the dynamics of the sample with the Cu tip diameter of 68 nm. More Cu cations can be injected into dielectrics. A straight-line-shaped CF appears at the bias of +50 V and the current of 14.4 μA. The widest diameter of the CF is around 25 nm and there is no gap between the Cu within the CF. **Figure 3**b shows that the diameter of the Cu tip increases to 210 nm. During the bias sweep, an obvious gradual growth of CF from the tip to the W electrode can be seen. Finally, a wide CF with the widest diameter of about 70 nm is formed, in the shape of a continuous inverted-cone directly connecting two electrodes. Meanwhile, the current reaches 14.6 μA. In the device with a larger active electrode, the CF is much wider and in the shape of a

continuous cone, which can maintain the status of connecting two electrodes for a long period and exhibit reasonably good retention. **Figure 3**c-e illustrates the ion migration and CF formation in this situation with large electrodes. **Figure 3**c is the starting state of the device, in which quite a few Cu atoms exist at the interface as a result of Cu atoms that remains from the last RESET cycle. When positive bias is applied, a large quantity of Cu cations is injected into SiO_2 simultaneously. The Cu cations drift towards W cathode, as shown in **Figure 3**d. Because of the lower mobility of Cu cations, they get reduced almost without traveling and pile up to form a wide CF. Due to the lower surface energy of the Cu in the large CF,[26] the Cu atoms prefer to stay close to each other and enable the filament to continuously grow to the cathode, as shown in **Figure 3**e. As a result, in devices with a wide active electrode, CF is wide and the morphology is continuous, leading to a stable LRS.

With the increase of Cu tip size, the diameter of CF in the SiO_2 film also increases. A comparison of our results with the existing literature,[14-16, 27-34] is shown in **Figure 4**. Except for several works performed in CBRAM devices with rather large electrodes,[14, 15, 27-29] almost all the previous works show an obvious trend that the CF size increases as the active electrode size increases, which is in good agreement with our work. Additionally, curved CF, cone-shaped CF, and straight-line-shaped CF are formed on the same device. Different CF shapes may be resulted from the different local grain boundary densities and/or defect densities of the SiO_2 electrolyte. Lu *et al.* have shown that the local mobility of cations can be affected by variations in the local defect density, defect energy profile and local electrochemical potentials.[16] Since Cu cations can transport more easily in a defect-rich region, or drift with lower energy needed, they preferably seek a path with the highest defect density and lowest electrochemical potentials. Therefore, various shapes of CF can be grown in the non-uniform sputtered SiO_2 film in our work.

To understand the CF growth dependence on the size of active electrode, we perform a quantitative analysis of the process that CF ions inject into the SiO_2 film during the SET operations. **Figure 5**a depicts the three-dimensional model for the SET process, in which a continuous cylinder- or cone-shaped CF grows from the active Cu tip towards the inert electrode. The two-dimensional equivalent plane is exacted from the model, and an orthogonal *x*-*y* coordinates system is established to describe the positions. According to the filament-based switching theory of CBRAM,[13, 35, 36] the filament first grows vertically until reaches the other

electrode, and then grows laterally after the SET occurs. In our *in-situ* SET operations, sweep biases were stopped immediately as the CF connected two electrodes, hence it is reasonable to approximate that only vertical growth of the CF happens in our experiments. The increasing volume of the CF in the vertical growth stage can be calculated by the accumulation of the reduced metal atoms.[37] Therefore, at time *t*, within the distance interval *dx*, the evolution of the CF volume $Q_{\Delta y}(x)$ can be expressed from the quantity of the charges in the reduction as

$$Q_{\Delta y}(x) = {}^{J}/_{Zq} \tag{1}$$

where *J* is the ion current density, *q* is the charge, *Z* is the number of the ions charged, which is 2 due to Cu^{2+} cations in this case. The current density *J* can be described by the Mott–Gurney ionic hopping current in solid electrolytes,[35, 38]

$$J = 2Zq \cdot N_i \cdot a_h \cdot f \cdot \exp(-\frac{E_A}{kT}) \cdot \sinh[E(x) \cdot \frac{Zqa_h}{2kT}] \tag{2}$$

where N_i is the concentration of the metal ions in the solid electrolytes, *f* is the attempt-to-escape frequency, E_A is the activation energy, *E(x)* is the electric field, *kT* is the thermal energy, and a_h is the effective hopping distance. Combining (1) and (2), the evolution rate of the CF volume is obtained as

$$Q_{\Delta y}(x) = 2N_i a_h f \exp(-\frac{E_A}{kT}) \sinh[E(x) \frac{Zqa_h}{2kT}] \tag{3}$$

Cu ion has low hopping mobility in SiO_2,[14, 16]. Thus, the concentration of metal ions N_i at the leading tip of the filament is determined by the hopping rate r_{hop}, which is directly related to the local electrical field. The local voltage difference is $\Delta V = E(x) \cdot \Delta y$, the ion concentration N_i can be described as[38, 39]

$$N_i = \alpha \cdot r_{hop} = \alpha \cdot f \cdot exp[-\frac{E_{A,hop} - \beta qE(x) \cdot \Delta y}{kT}] \tag{4}$$

where *f* is the attempt-to-escape frequency, $E_{A,hop}$ is the activation energy for cations hopping, α and β are factors in the simulation to modify the results. Thus, $Q_{\Delta y}(x)$ can be described as

$$Q_{\Delta y}(x) = 2\alpha a_h f^2 \, exp\left(-\frac{E_{A,hop} + E_A}{kT}\right) exp[\frac{\beta qE(x) \cdot \Delta y}{kT}] \, sinh[E(x) \cdot \frac{Zqa_h}{2kT}] \tag{5}.$$

The total volume of the CF at time *t* can be calculated as equation (6) below.

$$Q_{\Delta y,total} = \int_0^x 2\pi \cdot x \cdot Q_{\Delta y}(x) \cdot dx$$

$$= 4\pi\alpha a_h f^2 \, exp\left(-\frac{E_{A,hop} + E_A}{kT}\right) \int_0^x xexp[\frac{\beta qE(x) \cdot \Delta y}{kT}] \; sinh[E(x) \cdot \frac{Zqa_h}{2kT}] \, dx$$

(6)

All the physical parameters and their values used in the simulation are listed in Table 1.[36,39] Some of the parameters may be modified based on the experimental data. **Figure 5**b is the simulation results of electrical field distribution of CBRAM devices with the active electrode sizes of 30, 60, 68 and 210 nm, correspondingly to the experimental tip sizes. A CF nucleus with 5 nm height is assumed to have already grown in each device. +5 V bias is applied to the active electrode in the simulations. It shows that the Cu tip can greatly affect the electrical field distribution. Within the area contact to Cu tip, the electrical field is much larger than that out of the tip region; and the electrical field is strongest around the CF front, which is represent in red colors in the **Figure 5**b. **Figure 5**c shows the electric field distribution along the *x*-direction as a function of the size of active electrode. In the device with a smaller active electrode, electrical field affects narrower range of oxide electrolyte. But the electrical field at the central location is higher due to the curvature-induced effect of electrical filed concentration. Using the simulated electrical field distribution $E(x)$, we can calculate the total volume of the CF at time *t*. Because the CF is in the shape of a cylinder or a cone, the diameter (ϕ) of the growing CF at time *t* can be estimated by $\phi \propto \sqrt{Q_{\Delta y,total}}$, and the relationship between the CF size and the electrode size is obtained (black line in **Figure 5**d). The simulated line clearly shows that wider electrode will inject more ions and form wider CF. Because we have assumed that the CF evolution only occurs in the vertical direction from Cu towards W, the overall volume of the CF at SET switching can be viewed as a simple addition of the evolution volume at each time. Therefore, the size of the CF in an LRS device still exhibits a strong electrode-size-dependent trend, which is in good agreement with our *in-situ* experimental observation results, as compared between simulated black line and experimental data marked by blue stars in **Figure 5**d.

Conclusion

In summary, we observe the CF formation and dissolution processes in SiO_2-electrotlye-based CBRAM devices using *in-situ* TEM. Active electrodes with different sizes are used to investigate the size-dependent effects on the CF dimension. Our experimental results show that the shape, dimension and LRS retention of the CF is closely related to the active electrode size. With smaller active electrodes, due to the limited ion supply and high surface energy the ion clusters, the CF is thin and in the shape of discrete clusters. With larger electrodes, sufficient ion injection and lower surface energy result in a wide and continuous CF. This work provides a more complete understanding of the size parameters of the switching behavior, which may serve as a guide to improve the CBRAM performances, such as device scalability and reliability, etc.

Methods

Fabrication of CBRAM devices: We used a vertical-stacked memory structure of Cu/SiO_2/W in this study. The process started on a substrate of cleaned Si wafer with 300-nm-thick thermal grown SiO_2 as the isolation layer. First, an 85-nm-thick W layer was deposited as the bottom electrode (BE) by DC magnetron sputtering, and then the switching layer SiO_2 with the thickness of about ~30 nm was deposited by RF sputtering using a SiO_2 target in the mixed ambient of Ar and O_2. A 70-nm-thick Cu layer was deposited by DC magnetron sputtering and worked as top electrode (TE).

Ex-situ electrical measurements: Cu film was patterned into circular TEs with the diameter of 200 μm to characterize the Cu/SiO_2/W CBRAM devices. Cu TE was connected to a DC bias while W BE was grounded. The electrical measurement was performed by a Keithley 4200 semiconductor analyzer.

Preparation of the TEM specimen: The TEM specimens with the structure of SiO_2/W were prepared for the *in-situ* observation. The thicknesses of the SiO_2 and W layers were ~30 and 85 nm, respectively. The cross-sectional samples were made by a conventional method including cutting into 1 mm × 5 mm die, mechanical thinning and fixing onto a commercial TEM holder (Nanofactory^{TM} STM holder).

In-situ TEM measurements: The *in-situ* TEM experiments were performed in a Jeol JEM-2100F microscope. The Cu tip was prepared through electrochemical corrosion in KOH solution The Cu tip was contacted to SiO_2 film, acting as the movable active electrode of the CBRAM device. Electrical measurements were carried out by applying voltage to the movable probes with a Keithley 2400 analyzer and grounding the W BE via the holder. Images and videos were recorded by a CCD camera (2 frames/s).

ACKNOWLEDGMENTS

This work was supported by the Research Grant Council of Hong Kong (Grant No.: PolyU 252001/14E) and the Hong Kong Polytechnic University (1-ZE25 and 1-ZVDH). Xiaoyan Qiu thanks financial support by the National Natural Science Foundation of China (Grant No.:11274257). We appreciate the helpful discussion with Y. Zhao and Prof. J. Kang of Peking University, China.

ASSOCIATED CONTENT

Supporting Information is available free of charge on the ACS Publications website.

ex-situ switching characteristics of the $Cu/SiO_2/W$ devices, poor LRS retention of the $Cu/SiO_2/W$ devices during *in-situ* resistive switching; and videos of CF growth dynamics in the $Cu/SiO_2/W$ devices with different active electrode sizes.

AUTHOR INFORMATION

Corresponding Author

*Email: ychai@polyu.edu.hk

Table 1 Parameters and constants used in COMSOL simulation [36, 39]

Parameters/ Constant	**Values**
$\boldsymbol{a_h}$, $\Delta \boldsymbol{y}$	1 nm
$\boldsymbol{f}$	10^{13} Hz
$\boldsymbol{E_{A,hop}}$	1.2 eV
$\boldsymbol{E_A}$	0.5 eV
$\boldsymbol{\alpha}$, $\boldsymbol{\beta}$	0.5
T	298 K
Z	2
q	1.602×10^{-16} C
k	1.38×10^{-23} J/K

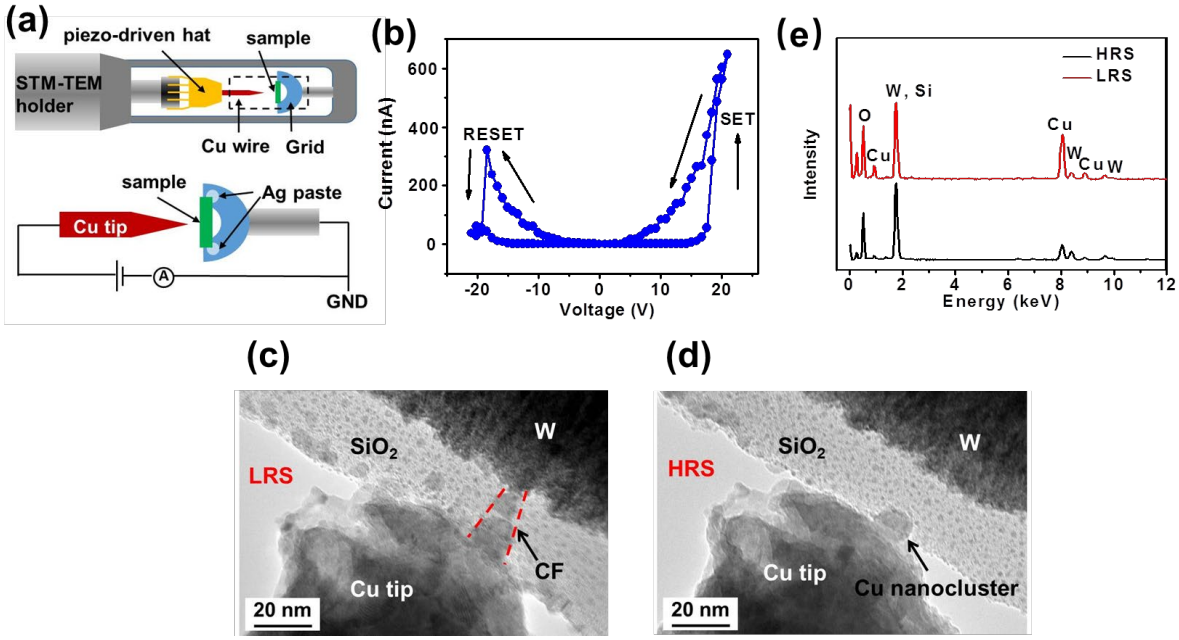

Figure 1. (a) The schematic of the *in-situ* TEM system set-up. (b) The *in-situ I-V* switching curve of the device with the arrows showing the voltage sweep direction. (c) The TEM image of the device in LRS and the CF is highlighted with red dash lines. The CF is in shape of inverted-cone comprising of a series of nanoclusters. (d) The TEM image of the same device after RESET operation to HRS with some residual Cu nanoclusters at the Cu/SiO_2 interface. (e) EDX analysis of the TEM specimen conducted at the LRS, and HRS, respectively. The EDX spectra were sequentially obtained at the CF region, which confirms the composition of the CF is Cu.

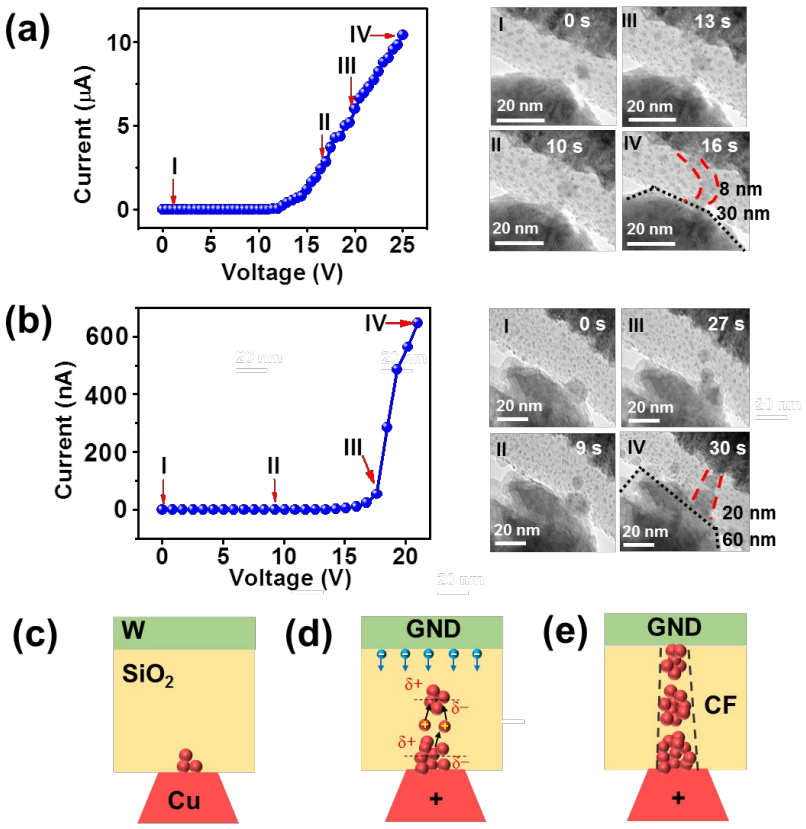

Figure 2. *In-situ I-V* curves at two sites of the same device with small active electrodes and the corresponding TEM images of the size-variable CF growth dynamics. The diameters of the Cu tip electrode and the CF are (a) 30 and 8 nm, and (b) 60 and 20 nm, respectively. (c) Schematic of the starting state with no bias of the device with small active electrode. (d) Schematic of the Cu cluster migration and CF growth in SET process. (e) Schematic of a thin and discrete-cluster-shaped CF grown in the device.

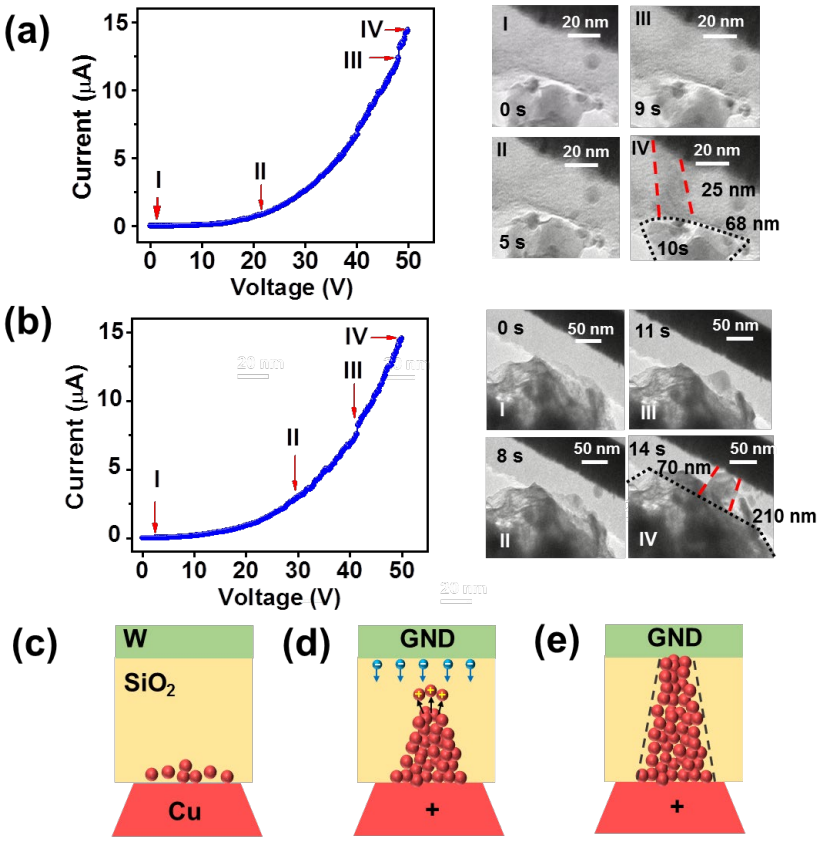

Figure 3. *In-situ I-V* curves of the same device with large active electrodes and the corresponding TEM images of the size-variable CF growth dynamics. The diameters of the Cu tip electrode and the CF are (a) 68 and 25 nm, and (b) 210 and 70 nm, respectively. (c) Schematic of the starting state with no bias of the device with large active electrode. (d) Schematic of the Cu migration and CF growth in SET process. (e) Schematic of a wide and continuous CF grown in the device.

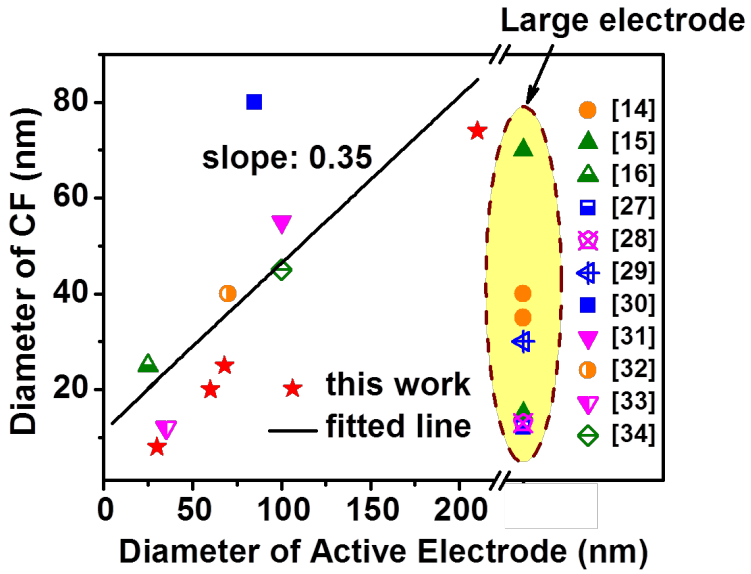

Figure 4. CF size dependence of active electrode size. Results of this work (red stars) are compared with literature works. The slope of the fitted line is 0.35.

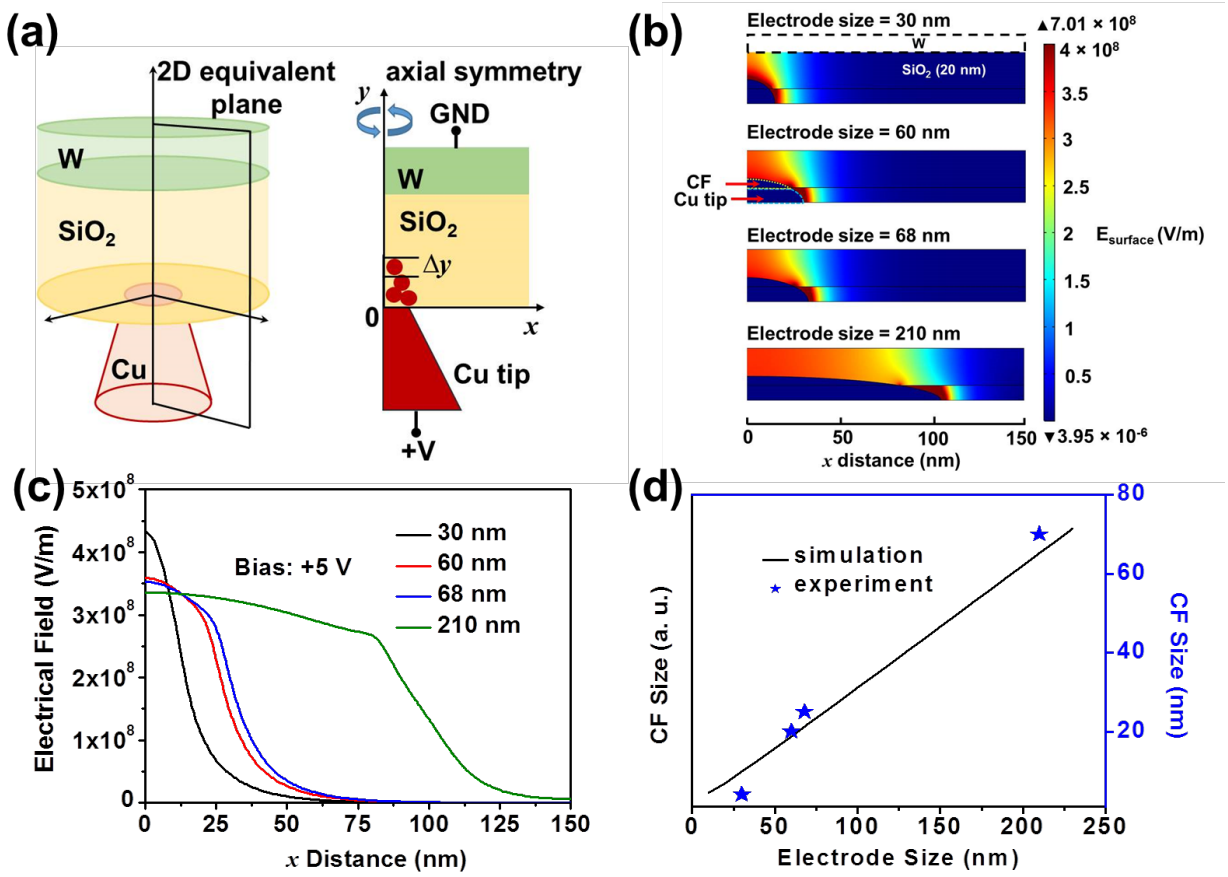

Figure 5. (a) Simulated geometry used in calculation. The axisymmetric geometry reduces the problem from three dimensions to two dimensions. (b) The simulation results of electrical field distributions in CBRAM devices with different active electrode size. A CF nucleus with 5 nm height is assumed to have already grown in each device. +5 V bias is applied to the active electrode (at bottom) in the simulations. The simulation tool is COMSOL software. (c) The electrical field distribution along the *x*-direction in CBRAM devices with different active electrode (Cu tip) size. (d) The simulation results of CF size as a function of electrode size, compared with TEM-observed results, which shows a good agreement.

References

(1) Waser, R.; Aono, M. Nanoionics-based resistive switching memories. *Nat. Mater.* **2007**, *6*, 833–840.

(2) Baek, I.G.; Lee, M.S.; Seo, S.; Lee, M.J.; Seo, D.H.; Suh, D.S.; Park, J.C.; Park, S.O.; Kim, H.S.; Yoo, I.K.; Chung, U.I. Highly scalable non-volatile resistive memory using simple binary oxide driven by asymmetric unipolar voltage pulses. *IEEE Int. Electron Devices Meet. Tech. Dig.* **2004**, 587–590.

(3) Wong, H.S.P.; Lee, H.Y.; Yu, S.; Chen, Y.S.; Wu, Y.; Chen, P.S.; Lee, B.; Chen, F.T.; Tsai, M.J. Metal–oxide RRAM. *Proc. of the IEEE*. **2012**, 100, 1951-1970.

(4) Wu, Y.; Chai, Y.; Chen, H. Y.; Yu, S.; Wong, H. –S. P. Resistive switching AlOx-based memory with CNT electrode for ultra-low switching current and high density memory application. *IEEE VLSI Technol. Symp. Dig*. **2011**, 26-27.

(5) Jo, S. H.; Kim, K. H.; Lu, W. High-density crossbar arrays based on a Si memristive system. *Nano Lett.* **2009**, *9*, 870-874.

(6) Goux, L.; Sankaran, K.; Kar, G.; Jossart, N.; Opsomer, K.; Degraeve, R.; Pourtois, G.; Rignanese, G.M.; Detavernier, C.; Clima, S.; Chen, Y.Y. Field-driven ultrafast sub-ns programming in W/Al_2O_3 /Ti/CuTe-based 1T1R CBRAM system. *IEEE VLSI Technol. Symp. Dig*. **2012**, 69-70.

(7) Jameson, J.R.; Blanchard, P.; Cheng, C.; Dinh, J.; Gallo, A.; Gopalakrishnan, V.; Gopalan, C.; Guichet, B.; Hsu, S.; Kamalanathan, D.; Kim, D. Conductive-bridge memory (CBRAM) with excellent high-temperature retention. *IEEE Int. Electron Devices Meet. Tech. Dig*. **2013**).

(8) Kund, M.; Beitel, G.; Pinnow, C.U.;Rohr, T.; Schumann, J.; Symanczyk, R.; Ufert, K.D.; Muller, G. Conductive bridging RAM (CBRAM): An emerging non-volatile memory technology scalable to sub 20nm. *IEEE Int. Electron Devices Meet. Tech. Dig*., **2005**.

(9) Chai, Y.; Wu, Y.; Takei, K.; Chen, H.Y.; Yu, S.; Chan, P.C.; Javey, A.; Wong, H.S.P. Nanoscale bipolar and complementary resistive switching memory based on amorphous carbon. *IEEE Trans. Electron Dev.* **2011**, *56*, 3933-3939.

(10) Yuan, F.; Wang, J.C.; Zhang, Z.; Ye, Y.R.; Pan, L.; Xu, J.; Lai, C.S. Hybrid aluminum and indium conducting filaments for nonpolar resistive switching of Al/AlO_x/indium tin oxide flexible device. *Applied Physics Express*. **2014**, *7*, 024204.

(11) Kozicki, M. N.; Balakrishnan, M.; Gopalan, C.; Ratnakumar, C.; Mitkova, M. Programmable metallization cell memory based on Ag-Ge-S and Cu-Ge-S solid electrolytes. *IEEE Non-Volatile Memory Tech. Symp.* **2005**, 83-89.

(12) Waser, R.; Dittmann, R.; Staikov, G.; Szot, K. Redox-based resistive switching memories–nanoionic mechanisms, prospects, and challenges. *Adv. Mat.* **2009**, *21*, 2632-2663,.

(13) Valov, I.; Waser, R.; Jameson, J. R.; Kozicki, M. N. Electrochemical metallization memories—fundamentals, applications, prospects. *Nanotechnol.* **2011**, *22*, 254003.

(14) Liu, Q.; Sun, J.; Lv, H.; Long, S.; Yin, K.; Wan, N.; Li, Y.; Sun, L.; Liu, M. Real-Time Observation on Dynamic Growth/Dissolution of Conductive Filaments in Oxide-Electrolyte-Based ReRAM. *Adv. Mat.* **2012**, *24*, 1844-1849.

(15) Yang, Y.; Gao, P.; Gaba, S.; Chang, T.; Pan, X.; Lu, W. Observation of conducting filament growth in nanoscale resistive memories. *Nat. Comm.* **2012**, *3*, 732.

(16) Yang, Y.; Gao, P.; Li, L.; Pan, X.; Tappertzhofen, S.; Choi, S.; Waser, R.; Valov, I.; Lu, W.D. Electrochemical dynamics of nanoscale metallic inclusions in dielectrics. *Nat. Comm.* **2014**, *5*, 4232.

(17) Liu, Q.; Long, S.; Lv, H.; Wang, W.; Niu, J.; Huo, Z.; Chen, J.; Liu, M. Controllable growth of nanoscale conductive filaments in solid-electrolyte-based ReRAM by using a metal nanocrystal covered bottom electrode. *ACS Nano*. **2010**, *4*, 6162-6168.

(18) You, B.K.; Kim, J.M.; Joe, D.J.; Yang, K.; Shin, Y.; Jung, Y.S.; Lee, K.J. Reliable Memristive-Switching Memory Devices Enabled by Densely-Packed Silver Nanocone Arrays as Electric-Field Concentrators. A*CS Nano*, **2016**, *10*, 9478-9488.,

(19) Park, J.; Lee, W.; Choe, M.; Jung, S.; Son, M.; Kim, S.; Park, S.; Shin, J.; Lee, D.; Siddik, M.; Woo, J. Quantized conductive filament formed by limited Cu source in sub-5nm era. *IEEE Int. Electron Devices Meet. Tech. Dig.* **2011**, 3-7.

(20) Park, J.; Jung, S.; Lee, W.; Kim, S.; Shin, J.; Lee, D.; Woo, J.; Hwang, H. Improved switching variability and stability by activating a single conductive filament. *IEEE Electron Dev. Lett.*, **2012**, *33*, 646-648.

(21) Li, L.; Zhu, Z.; Wang, T.; Currivan-Incorvia, J. A.; Yoon, A.; Wong, H.-S. P. BEOL Compatible Graphene/Cu with Improved Electromigration Lifetime for Future Interconnects. IEEE *IEDM Tech. Dig.* **2016**.

(22) Zhao, Y.; Liu, Z.; Sun, T.; Zhang, L.; Jie, W.; Wang, X.; Xie, Y.; Tsang, Y.H.; Long, H.; Chai, Y. Mass Transport Mechanism of Cu Species at the Metal/Dielectric Interfaces with a Graphene Barrier. *ACS nano*, **2014**, *8*, 12601-12611.

(23) Yang, Y.; Lu, W. Nanoscale resistive switching devices: mechanisms and modeling. *Nanoscale*, **2013**, *5*, 10076-10092.

(24) Takahashi, Y.; Kudo, M.; Fujiwara, I.; Shimuta, M.; Ohba, K.; Arita, M. Visualization of Conductive Filament during Write and Erase Cycles on Nanometer-Scale ReRAM Achieved by In-Situ TEM. *2015 IEEE International Memory Workshop (IMW)*, **2015**, 1-4.

(25) Guy, J.; Molas, G.; Vianello, E.; Longnos, F.; Blanc, S.; Carabasse, C.; Bernard, M.; Nodin, J.F.; Toffoli, A.; Cluzel, J.; Blaise, P. Investigation of the physical mechanisms governing data-retention in down to 10nm nano-trench Al_2O_3/CuTeGe conductive bridge RAM (CBRAM). *IEEE Int. Electron Devices Meet. Tech. Dig.* **2013**, 30.2.1-30.2.4.

(26) Tsuruoka, T.; Terabe, K.; Hasegawa, T.; Aono, M. Forming and switching mechanisms of a cation-migration-based oxide resistive memory. *Nanotechnology*, **2010**, *21*, 425205.

(27) Sun, J.; Liu, Q.; Xie, H.; Wu, X.; Xu, F.; Xu, T.; Long, S.; Lv, H.; Li, Y.; Sun, L.; Liu, M. In situ observation of nickel as an oxidizable electrode material for the solid-electrolyte-based resistive random access memory. *Appl. Phys. Lett.* **2013**, *102*, 053502.

(28) Arita, M.; Takahashi, A.; Ohno, Y.; Nakane, A.; Tsurumaki-Fukuchi, A.; Takahashi, Y. Switching operation and degradation of resistive random access memory composed of tungsten oxide and copper investigated using in-situ TEM. *Sci. Rep.* **2015**, *5*, 17103.

(29) Nayak, A.; Wang, Q.; Itoh, Y.; Tsuruoka, T.; Hasegawa, T.; Boodhoo, L.; Mizuta, H.; Aono, M. Position detection and observation of a conducting filament hidden under a top electrode in a Ta_2O_5-based atomic switch. *Nanotech.* **2015**, *26*, 145702.

(30) Choi, S.J.; Park, G.S.; Kim, K.H.; Cho, S.; Yang, W.Y.; Li, X.S.; Moon, J.H.; Lee, K.J.; Kim, K. In Situ Observation of Voltage-Induced Multilevel Resistive Switching in Solid Electrolyte Memory. *Adv. Mat.* **2011**, *23*, 3272-3277.

(31) Peng, C.N.; Wang, C.W.; Chan, T.C.; Chang, W.Y.; Wang, Y.C.; Tsai, H.W.; Wu, W.W.; Chen, L.J.; Chueh, Y.L. Resistive switching of Au/ZnO/Au resistive memory: an in situ observation of conductive bridge formation. *Nanoscale Res. Lett.* **2012**, *7*, 599.

(32) Tian, X.; Wang, L.; Wei, J.; Yang, S.; Wang, W.; Xu, Z.; Bai, X. Filament growth dynamics in solid electrolyte-based resistive memories revealed by in situ TEM. *Nano Res.*, **2014**, *7*, 1065-1072.

(33) Hubbard, W.A.; Kerelsky, A.; Jasmin, G.; White, E.R.; Lodico, J.; Mecklenburg, M.; Regan, B.C. Nanofilament Formation and Regeneration During Cu/Al2O3 Resistive Memory Switching. *Nano Lett.* **2015**, *15*, 3983-3987.

(34) Jang, M.H.; Agarwal, R.; Nukala, P.; Choi, D.; Johnson, A.C.; Chen, I.W.; Agarwal, R. Observing Oxygen Vacancy Driven Electroforming in Pt–TiO2–Pt Device via Strong Metal Support Interaction. *Nano Lett.* **2016**, *16*, 2139-2144.

(35) Yu, S.; Wong, H. -S. P. Compact modeling of conducting-bridge random-access memory (CBRAM). IEEE *Trans. Electron Dev.* **2011**, *58*, 1352-1360.

(36) Zhao, Y. D.; Hu, J. J.; Huang, P.; Yuan, F.; Chai, Y.; Liu, X. Y.; Kang, J. F. A Physics-Based Compact Model for Material- and Operation-Oriented Switching Behaviors of CBRAM. IEEE *IEDM Tech. Dig.* **2016**.

(37) Guo, H.X.; Gao, L.G.; Xia, Y.D.; Jiang, K.; Xu, B.; Liu, Z.G.; Yin, J. The growth of metallic nanofilaments in resistive switching memory devices based on solid electrolytes. *Appl. Phys. Lett.* **2009**, *94*, 153504.

(38) Mott N F, Gurney R W, Electronic Processes in Ionic Crystals. London, U.K.: Oxford Univ. Press, **1948**.

(39) Qin, S.; Liu, Z.; Zhang, G.; Zhang, J.; Sun, Y.; Wu, H.; Qian, H.; Yu, Z. Atomistic study of dynamics for metallic filament growth in conductive-bridge random access memory. *Phys. Chem. Chem. Phys.* **2015**, *17*, 8627-8632.